URSI AP-RASC 2019, New Delhi, India, 09 - 15 March 2019

Planar Metamaterial with Simultaneous Giant Circular Dichroism and Wavefront Control

He-Xiu Xu [(1,2)], Guangwei Hu[(1)], Lei Han[(1)], Ying Li[(1)], Cheng-Wei, Qiu*[(1)]
(1) Department of Electrical and Computer Engineering, National University of Singapore, Singapore 117583, Singapore
(2) Air force Engineering University, Xi'an, 710051, China

Abstract

Achieving simultaneous polarization and wavefront control is extremely crucial in vast optical systems. Here, a new strategy is proposed by incorporating the constructive and destructive interferences to achieve the giant circular dichroism based on the theory of Pancharatnam-Berry phase. By fulfilling a general criterion we established, the meta-atom features total absorption at one helicity of circularly-polarized (CP) wave while left the other totally reflected, enabling a spin-selective asymmetric diode-like reflections. On the basis of our finding, a single-layer metasurfaces with spatially rotated anisotropic meta-atoms were proposed for wavefront control: that is to accomplish the spin-selective Bessel-beam wavefront at right-handed CP wave while low radar cross section (RCS) at left-handed CP wave. For verifications, these metasurfaces were numerically and experimentally characterized at microwave frequencies. Numerical and experimental results agree well, illustrating elegant bifunctionalities of helicity-dependent non-diffractive propagation and wide-angle RCS reduction for one metasurface, while multiple vortices with versatile beam numbers and spiral wavefront for the other. Our findings offer a new avenue for CP asymmetric reflections without cascading bulky optical components.

1. Introduction

Metasurfaces[1], a planar equivalent of metamaterials comprising a set of subwavelength resonant meta-atoms, have triggered enormous interest due to their low loss, easy fabrication and extreme capabilities in manipulating electromagnetic (EM) waves. Using metasurfaces to control amplitudes and phases of transmissions/reflections and thus shape complex wavefront has intrigued appealing interest in both science and engineering community due to their large applications in modern microwave/optical communication systems. Moreover, the simultaneous amplitude and phase control has also been realized in a single flat plate[2]. Nevertheless, all predefined functions were actualized under certain polarizations, which undoubtedly limited considerably the degree of freedom for full wave control. Such issue compels us to connect the feature of both phase and polarization which is another crucial characteristic of EM wave, and manipulation of which is of utmost importance in photonic research.

The simultaneous polarization and phase manipulation for wavefront control is challenging in practice. Traditional methodology is combining linear polarizers, waveplates, and specific phase retarders (prisms and lenses, etc). Such strategy of cascading optical devices facilitates bulky systems, low efficiency and worsened performances. Although chiral metamaterials [3] were believed to be a promising candidate for polarization manipulation, the periodic structures in homogenous profile generally restricted their capability in shaping desired wavefronts. The emerging helicity-dependent wavefront control has been realized by using Pancharatnam-Berry (PB) phases launched by circularly-polarized (CP) waves[4]. However, the functionalities under left-handed (LCP) and right-handed (RCP) CP waves are essentially locked together due to the inverse phase profile flipping as the spin state of the incident wave changes. To date, the physics and criterion for spin-selective absorption is still in infancy and remains elusive.

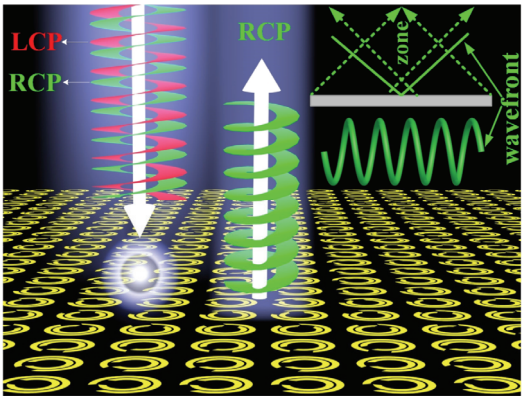

Figure 1. Schematic illustration of the functionality of proposed metasurface with simultaneous giant circular dichroism and wavefront control.

Here, we proposed a novel strategy to enable a new paradigm to individually modulate EM wavefronts by flipping the spin states of CP waves based on constructive and destructive interferences. Following the established criterion, the basic building block is designed even without introducing chirality. The physics for the diodelike asymmetric reflections (circular dichroism) lies in the destructive or constructive interference induced by the 180° and 0° phase difference between r_{RR} or r_{LL} of two split ring resonators (SRRs) with a mutual twist of 45°. For applications in wavefront control, a proof-of-concept metasurface using a set of spatially rotated meta-atoms was designed by taking the feature of asymmetric CP reflections. The metasurface exhibits non-diffracting reflective propagation (Bessel beam) at RCP state, see Fig.

1. At LCP state, low radar cross section (RCS) and suppressed pencil beams are obtained due to the total absorptions of LCP wave. In contrast to previous designs, our approach features monolayer, definite physics and easy design. These findings offer a new methodology to implement novel photonic devices for a variety of applications in optical diodes, circulators, and isolators.

2. Principle and criterion for spin-selective diodelike asymmetric reflections

The basic meta-atom we proposed is a metallic-insulator-metallic reflection structure backed by a complete metallic ground, see Fig. 2(a). The top metallic structure is composed of two split ring resonators (SRRs) with a mutual twist of ψ=45°. For convenience, the external big and internal small SRR are termed as SRR_1 and SRR_2. The composite meta-atom and backed ground are separated by a F4B dielectric spacer with a dielectric constant of ε_r=4.5, thickness of h=3 mm and loss tangent of δ=0.025. By individually controlling the geometrical parameters of SRR_1 and SRR_2, arbitrary phase difference $\Delta\varphi=\varphi_1-\varphi_2$ can be engineered between two reflections of r_{RR1} and r_{RR2}, or those of r_{LL1} and r_{LL2} under RCP or LCP wave stimulation.

To begin with, assume a plane CP wave is normally incident on the meta-atoms containing bare SRR_1 or SRR_2 with a common rotation angle Φ. Similar to V shape antenna, both SRR_1 and SRR_2 exhibit symmetric and asymmetric mode along and perpendicular to the symmetry axis under plane CP wave excitation. This is because any CP wave can be decoupled into double orthogonal linearly polarized (LP) components along aforementioned two directions. At these resonances, several reflection zeros will manifest on r_{LR} and r_{RL} spectra. Therefore, the reflective field at RCP state regardless of the negligible cross-polarization component can be simplified as

$$\begin{aligned} E_{R1} &= |r_{RR1}|E_i e^{i(\varphi_1+2\Phi)} \\ E_{R2} &= |r_{RR2}|E_i e^{i(\varphi_2+2\Phi\pm2\psi)} \end{aligned} \quad (1).$$

In a similar manner, the reflective beam under normal illumination of a plane LCP wave can be immediately obtained as

$$\begin{aligned} E_{L1} &= |r_{LL1}|E_i e^{i(\varphi_1-2\Phi)} \\ E_{L2} &= |r_{LL2}|E_i e^{i(\varphi_2-2\Phi\mp2\psi)} \end{aligned} \quad (2).$$

Then, the reflections of proposed composite meta-atom regardless of mutual coupling between SRR_1 and SRR_2 are synthesized as

$$\begin{aligned} E_{R\text{com}} &= E_{R1}/2 + E_{R2}/2 \\ &= |r_{RR1}|E_i e^{i(\varphi_1+2\Phi)}/2 + |r_{RR2}|E_i e^{i(\varphi_2+2\Phi\pm2\psi)}/2 \\ E_{L\text{com}} &= E_{L1}/2 + E_{L2}/2 \\ &= |r_{LL1}|E_i e^{i(\varphi_1-2\Phi)}/2 + |r_{LL2}|E_i e^{i(\varphi_2-2\Phi\mp2\psi)}/2 \end{aligned} \quad (3).$$

Since it is easy to achieve $|r_{RR1}|\approx|r_{RR2}|\approx1$ and $|r_{LL1}|\approx|r_{LL2}|\approx1$ in a reflection scheme, then the left φ_1, φ_2, Φ, and ψ play a determinant role to obtain CP asymmetric reflections. To minimize $E_{L\text{com}}$ while simultaneously maximize $E_{R\text{com}}$, the following criterion should be fulfilled.

$$\begin{aligned} \varphi_1-\varphi_2\mp2\psi&=0 \\ \varphi_1-\varphi_2\pm2\psi&=180 \end{aligned} \quad (4).$$

From Eq (4), we immediately derive the exclusive solution of $\Delta\varphi=\varphi_1-\varphi_2=90°$ and $\psi=45°$, which is a general criterion for diodelike circular dichroism. Above phase requirement is only related to the structures and dimensions of the meta-atom. Using above criterion, we achieve full reflection of RCP wave through constructive interference while total suppression of LCP wave through destructive interference. Similar criterion of $\Delta\varphi=\varphi_1-\varphi_2=90°$ and $\psi=-45°$ can be derived for full and zero reflection of LCP and RCP waves. Furthermore, the amplitude of all four reflections in Jones matrix can be tuned by cautiously choosing an appropriate ψ.

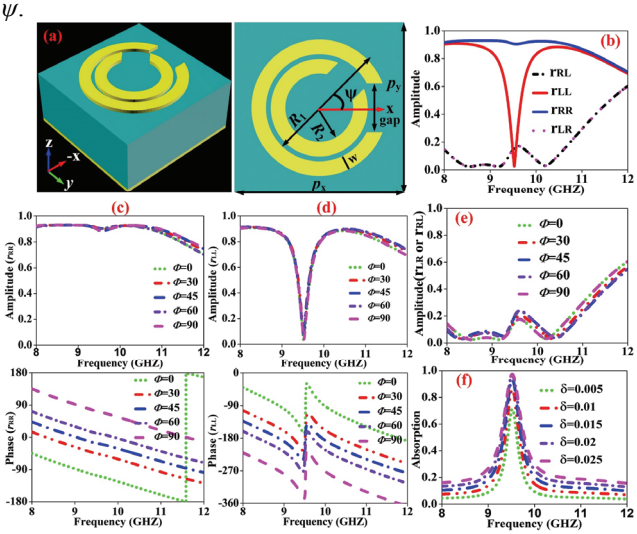

Figure 2. Characterization of the basic meta-atom with asymmetric reflections. (a) Illustration of the topology and structure parameters. (b) FDTD simulated reflection spectra under normally illuminated LCP and RCP plane wave. FDTD simulated reflection amplitude (top panel) and phase (bottom panel) spectra of (c) r_{RR} and (d) r_{LL} as a function of rotational angle Φ. (e) FDTD simulated reflection amplitude of r_{LR} and r_{RL} varying as Φ. (f) Absorption spectrum calculated by $a_L = 1 - r_{LL}^2 - r_{RL}^2$ varying as δ. The geometrical parameters are detailed as R_1=2.2 mm, R_2=1.4 mm, w=0.6 mm, p_x=p_y=7 mm, ψ=45° and the gap width of the inner and outer ring is 1.5 and 2 mm, respectively.

For verification, we characterize proposed meta-atom designed following above criterion using finite - difference - time - domain (FDTD) solutions. As expected in Fig. 2(b), the handedness of reflection beams preserved for both LCP and RCP wave incidence while the cross-polarization components are maintained extremely low. Moreover, the reflection amplitude $|r_{RR}|$ remains above 0.71 across the entire observed band while $|r_{LL}|$ undergoes a sudden drop with magnitude approaching null at 9.5 GHz, enabling a maximum extinction ratio of $|r_{RR}|/|r_{LL}|$=33.3. Moreover, r_{RR} manifests almost constant amplitude and ideal PB phase with reflection phase twice the Φ, see Fig. 2(c). Such orientation-immune high-rate reflections and dispersionless PB phase are crucial for high-efficiency wavefront control. Nevertheless, the ideal PB phase does

not hold for r_{LL} near the perfect absorption region in Fig. 2(d). Similar constant reflections immune to Φ also hold for r_{RL} and r_{LR}, see Fig. 2(e). It should be emphasized that the spin-selective asymmetric reflection is not induced by the loss of dielectric boards, see Fig. 2(f) where the high absorptions sustained even if the loss tangent δ reaches up to 0.005. Despite this, the reflection rate of $|r_{RR}|$ is indeed slightly affected by δ and more than 95% of efficiency is expected when δ=0.005.

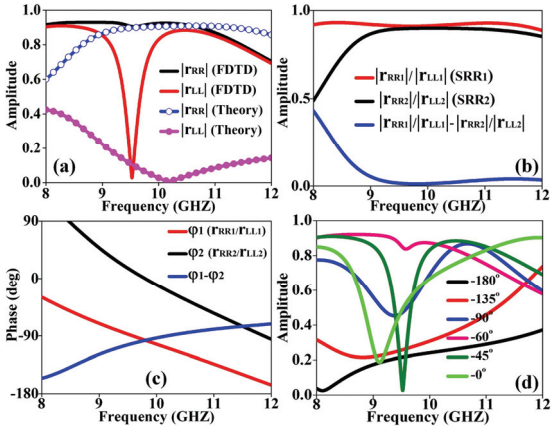

Figure 3. Illustration of the mechanism for diodelike asymmetric reflections. (a) Comparison of FDTD simulated and theoretically calculated reflection spectrum of $|r_{RR}|$ and $|r_{LL}|$. In theoretical calculations, $|r_{RR}|$ and $|r_{LL}|$ are calculated by $|r_{RR}|=|r_{RR1}|\cos(\varphi_1)+|r_{RR2}|\cos(\varphi_2+2\psi)$ and $|r_{LL}|=|r_{LL1}|\cos(\varphi_1)+|r_{LL2}|\cos(\varphi_2-2\psi)$. FDTD simulated reflection (b) amplitude and (c) phase spectrum of a meta-atom with bare SRR_1, SRR_2 and their difference. (d) The variation of $|r_{LL}|$ as a function of the twist angle ψ.

We now further verify the physical mechanism of diodelike asymmetric reflections based on the established criterion. As expected in Fig. 3(a), the FDTD and theoretically calculated reflection spectra are in reasonable agreement, verifying the physics of destructive and constructive interference. Such proposal finds strong support from Fig. 3(b) and 3(c), where the reflection spectra of SRR_1 and SRR_2 are individually characterized through FDTD simulations. The amplitudes $|r_{RR1}|$ and $|r_{LL1}|$ of SRR_1 are almost the same as those ($|r_{RR2}|$ and $|r_{LL2}|$) of SRR_2 while the phase difference $\Delta\varphi=\varphi_1-\varphi_2$ between them is near 90°. Such condition is exactly the criterion set by Eq. (4). The deviation between theory and FDTD simulations especially for the wideband absorption in the latter case is attributable to the coupling between two closely spaced SRRs. As expected in Fig. 3(d), the $|r_{LL}|$ can be continuously modulated by controlling twist angle of ψ within -180°~0°, coinciding well the conclusion predicted by theory. The same conclusion can be drawn for r_{RR} by engineering ψ within 0°~180°.

As depicted in Fig. 4, a remarkable diodelike asymmetric absorption is again clearly appreciated from a_{LL} and a_{RR} at LCP and RCP state in both xz or yz incident plane. Moreover, the near-unity and null asymmetric absorption in LCP and RCP channel preserves over a wide range of incidences. Even when incidence reaches 80°, the absorption of a_{LL} is still larger than 68% and 76% in xz and yz plane. The absorption at two states still maintains a high contrast (>50%) for incidence up to 65°, indicating a robust wide-angle absorption behavior. The slight deviation of absorption behavior a_{LL}, i.e., red and blue frequency shift in xz and yz plane at large incident angles, is attributable to the simultaneous breaking of mirror and rotational symmetry. Such high-contrast incidence-insensitive diodelike reflections are highly beneficial for applications in single-mode devices of CP light.

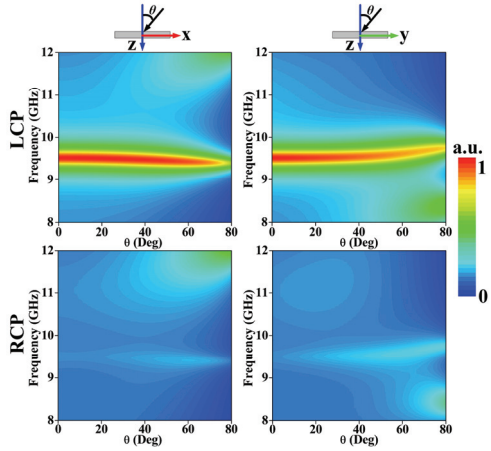

Figure 4. FDTD simulated absorption spectra of a_L (top row) and $a_R=1-r_{RR}^2-r_{LR}^2$ (bottom row) at LCP and RCP state as a function of incident angle θ and frequency, when incident wave propagates in the xz-plane (left panel) and yz-plane (right panel), respectively.

3. Bessel beam and RCS reduction

In what follows, we will demonstrate the capability of using such CP asymmetric reflections to engineer distinct wavefront control. The metadevice is engineered to generate non-diffractive Bessel beams. The metasurface targeting at 10 GHz is composed of 31*31 meta-atoms and occupies a total area of 217*217 mm^2. To form the diffraction-free focusing wavefront at RCP state, the imparted phase should follow $\varphi_{Axicon}=\sin(\tan^{-1}(\frac{R}{F}))*\frac{2\pi}{\lambda}*\sqrt{x^2+y^2}$ with F=100 mm being the long depth of focus and R=108.5 mm the half of axicon aperture, see the 2D hyperbolic phase profile and liner phase profile along y=0 mm (dashed) shown in Fig. 5(a). Then, the metasurface layout can be easily mapped out by spatially varying orientations of meta-atoms with constant geometrical parameters, see Fig. 5(b). For experimental verication, a proof-of-prototype sample is fabricated using printed circuit board (PCB) technique and the spin-selective non-diffracting reflection and wide-angle RCS reduction is evaluated in a microwave anechoic chamber, see Methods for experimental details.

As shown in Fig. 5(c), distinctly different behavior is clearly seen under two opposite-helicity channels. For RCP channel, we observe a non-diffracting propagation (Bessel beams) behavior along z axis across a desirable distance and a wide range of frequencies. However, in sharp contrast, weak and dispersed energy distributions with diverged field are inspected for LCP channel. Moreover, the near fields even approach null across the entire plane at

9.5 GHz, where the extinction ratio, calculated as the scale of maximum power of two channels, is evaluated more than 50. Such desirable distinct functions are attributable to the diode-like asymmetric reflections of utilized meta-atoms. From Fig. 5(d) and Fig. 5(e), a reasonable agreement of results is observed between simulations and measurements. As expected, the energy is mainly confined around the optical axis and propagates along the axis over considerable distance (approximate 75 mm by 3 dB energy attenuation) without diffraction. The half-power beamwidth in transverse plane is about 15 mm and remains almost constant as frequency varies, see Fig. 5(e), where good Bessel-like profiles of electric fields with first zero are clearly observed. The slightly shifted beam toward large distances along z axis as frequency increases is because the electrically shortened aperture at low frequencies makes our metadevice less efficient for long-focal-length imaging. As expected in Fig. 5(f), the backward RCS has been significantly reduced more than 7 dB across 8~12 GHz. This is especially true for that near 9.5 GHz where the RCS reduction even reaches -20.7 dB, also see the 3D scattering patterns at 9.5 GHz in the inset. Most importantly, the low-RCS behavior is insensitive to the incidence and the RCS reduction is preserved better than -6 dB even at θ=45°.

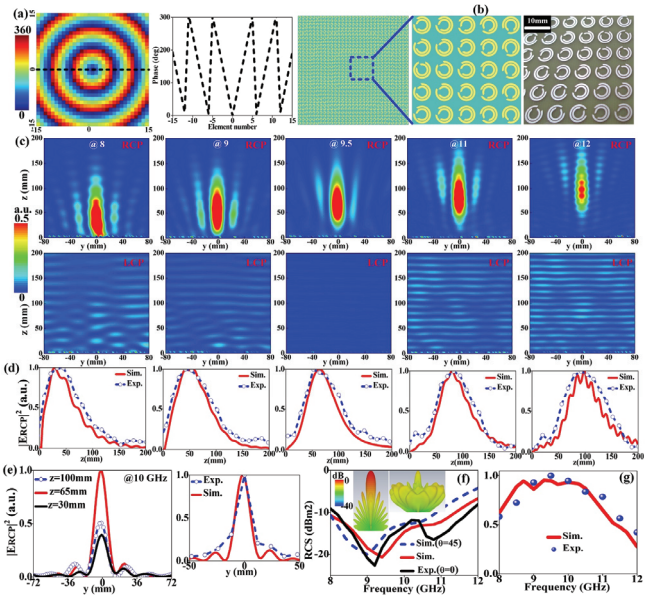

Figure 5. Characterization of the metasurface Bessel-beam generator. (a) Phase distribution across the axicon aperture and centre line. (b) Metasurface layout and zoom-in-view of the fabricated prototype. (c) FDTD simulated E-field intensity distributions at five typical frequencies of 8, 9, 9.5, 11 and 12 GHz under plane RCP (top row) and LCP (bottom row) wave illumination. Near-field E_{RCP} intensity at RCP state (d) along the propagating direction (z axis) at x=0 mm and (e) at various yz planes with z varying from z=30 to z=125 mm away from the metadevice. (f) Normalized far-field RCS reduction spectrum to PEC ground of the same size and (g) near-field E_{RCP} intensity spectra at the focal point (maximum intensity) under illumination of LCP and RCP waves. The inset to Fig. 5(f) shows the 3D scattering patterns of the metasurface and PEC of the same size at 9.5 GHz. Here, all fields are normalized against its maximum.

Finally, we show in Fig. 5(g) the E-field intensity spectra at the focal point to quantitatively evaluate the working bandwidth. As expected, the E-field intensity reaches its maximum around f_0=10 GHz, indicating the best capability of Bessel beam generation. However, the capability becomes deteriorative as frequencies go far beyond f_0 since the phase profile no longer strictly follows the required dispersive hyperbolic-phase. The working bandwidth characterized by half-power decay is about 3.4 GHz (8~11.4 GHz), corresponding to a fractional bandwidth of 34%. The slight deviations between simulations and measurements are attributable to the tolerances inherent in sample fabrication and measurements, i.e., inaccurate alignment of metasurface and feed horn, and imperfect non-planar incoming wavefront.

4. Conclusion

To sum up, we have proposed a new type of meta-atom with CP asymmetric diode-like reflections, i.e., selectively reflect RCP waves with high efficiency of 95% while totally absorber LCP waves, based on new physics of constructive and destructive interference. Of particular relevance is the established criterion which affords a general guideline to engineer arbitrary extinct ratio of CP waves using arbitrary structures. For verification, a diffraction-free Bessel generator is numerically and experimentally characterized. Results show that the metasurfaces exhibit wide-angle insensitive absorption behavior under plane LCP wave excitation while manifest desired spatial wavefronts under RCP wave stimulation. Our strategy, opens an avenue to flexibly control both the helicity and phases of CP light in a prescribed manner by decoupling the LCP and RCP channel due to their unprecedented ability.

5. Acknowledgements

This work was supported by the National Natural Science Foundation of China (61501499); Youth Talent Lifting Project of the China Association for Science and Technology (17-JCJQ-QT-003); National Research Foundation of Singapore (NRF-CRP15-2015-03); Key Program of Natural Science Foundation of Shaanxi Province (2017KJXX-24); China Scholarship Fund (20173059).

6. References

1. R. C. Devlin, A. Ambrosio, N.A. Rubin, JPB Mueller, F. Capasso, "Arbitrary spin-to–orbital angular momentum conversion of light," *Science* **358**, 2018, pp. 896–901.

2. L. Liu , X. Zhang , M. Kenney, X. Su , N. Xu, C. Ouyang, Y. Shi, J. Han, W. Zhang, and S. Zhang, "Broadband metasurfaces with simultaneous control of phase and amplitude," *Adv. Mater.* **26**, 2014, pp. 5031-5036.

3. Y. Zhao, M.A. Belkin, A. Alù, "Twisted optical metamaterials for planarized ultrathin broadband circular polarizers," *Nat. Commun.* **3**, 2012, p. 870.

4. D. Wen, F. Yue, G. Li, G. Zheng, K. Chan, S. Chen, *et al*, "Helicity multiplexed broadband metasurface holograms," *Nat. Commun.* **6** 2015, p. 8241.